Inorganic Chemistry

Article

pubs.acs.org/IC

$(IP)_2Ga^{III}$ Complexes Facilitate Net Two-Electron Redox Transformations (IP = α-Iminopyridine)

Chelsea D. Cates,[‡] Thomas W. Myers,[‡] and Louise A. Berben*

Department of Chemistry, University of California—Davis, Davis, California 95616, United States

Supporting Information

ABSTRACT: Reaction of $M^+[(IP^{2-})_2Ga]^-$ (IP = iminopyridine, M = Bu_4N, **1a**; $(DME)_3Na$, **1b**) with pyridine *N*-oxide affords two-electron-oxidized $(IP^-)_2Ga(OH)$ (**2**) in reactions where the product outcome is independent of the cation identity, M^+. In a second example of *net* two-electron chemistry, outer sphere oxidation of $M^+[(IP^{2-})_2Ga]^-$ using either 1 or 2 equiv of the one-electron oxidant ferrocenium afforded $[(IP^-)_2Ga]^+$ (**3**) in either 44 or 87% yield, respectively. Reaction with 1 equiv of TEMPO, a one-electron oxidant, afforded the two-electron-oxidized product $(IP^-)_2Ga$-(TEMPO) (**4**). Reduction of 2IP by 3Na and subsequent reaction with $GaCl_3$ yielded a 1:1 mixture of $(IP^-)_2GaCl$ and **1**. Most remarkably, all of these reactions are overall two-electron processes and only the $(IP^-)_2GaX$ and $[(IP^{2-})_2Ga]^-$ oxidation states are thermodynamically accessible to us. Analogous aluminum chemistry previously afforded either one-electron or two-electron reactions and mixed-valent states. The thermodynamic accessibility of the mixed-valent states $(IP^{2-})(IP^-)E$, where E = Al or Ga, can be compared using cyclic voltammetry measurements. These measurements indicated that the mixed-valent state $[(IP^{2-})(IP^-)Ga]^+$ is not significantly stabilized with respect to disproportionation on the time scale of the electrochemistry experiment. The electrochemically observed differences in thermodynamic stability of the mixed-valent state $[(IP^{2-})(IP^-)E]^+$ can be rationalized by the observation that the dihedral angle between the ligand planes containing the π-system of IP is roughly 5° larger in all gallium complexes compared with aluminum analogs. Presumably, a larger dihedral angle provides weaker electronic coupling between the π-systems of IP via the E−X σ* orbital. Alternatively, the observed difference may be a result of the "inert pair effect": a contracted Ga component in the E−X σ* orbital would also afford weaker electronic coupling.

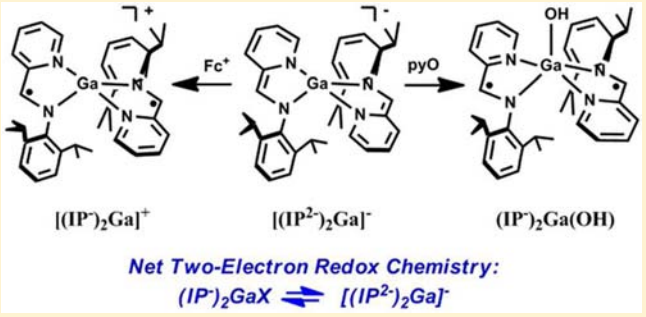

INTRODUCTION

A preference for two-electron chemistry is associated with the platinum group metals, such as Pt, Pd, Ir, and Rh, and enables their central role in transition-metal catalysis.[1] The impetus to develop predictably net two-electron redox reactions for the main group elements derives from two main goals. The prospect of employing the inexpensive and abundant main group elements for catalysis is appealing,[2] as is a new route to functionalization of metals that are often inert to classical substitution chemistry due to their high Lewis acidity.

Low valent compounds of group 13 have been shown to undergo two electron redox transformations when the +1 to +3 redox couple is harnessed. For example, complexes of the form $E[\{N(Dipp)C(Me)\}_2CH]$ [E = Al, Ga, Dipp = 2,6-bis(1-methylethyl)phenyl] can undergo reaction with a wide variety of substrates. In the case of gallium, $Ga[\{N(Dipp)C(Me)\}_2CH]$ is oxidized by N_2O or S_8 to form $\{YGa[\{N(Dipp)C(Me)\}_2CH]\}_2$ (Y = O or S).[3] The aluminum analog $Al[\{N(Dipp)C(Me)\}_2CH]$ reacts with O_2 to afford $\{OAl[\{N(Dipp)C(Me)\}_2CH]\}_2$, while the reaction with 1 equiv of S_8 leads to formation of $\{S_3Al[\{N(Dipp)C(Me)\}_2CH]\}_2$.[4] The products from the reactions of the aluminum complexes with oxygen and sulfur are not direct analogs, but two-electron oxidation of the metal is reported in each case. Lastly, complexes of both Ga(I) and Al(I) have been shown to undergo reactions with bulky azides to form transient metal imide intermediates that activate C−H bonds.[5,6]

Ligand-based redox chemistry has become more highly recognized in recent years, but in general, this chemistry resembles the redox characteristics of first row transition elements: influenced by substrate, the chemistry can generally afford isolable one- or two-electron-oxidized or -reduced products. Work by Heyduk and co-workers with tantalum complexes of the redox-active tris(amido) $[NNN^{cat}]^{3-}$ ligand {$[NNN^{cat}]^{3-}$ = bis(2-isopropylamino-4-methoxyphenylamine)} have led to substrate controlled one- and two-electron oxidation of $\{[NNN^{cat}]TaCl_2\}$ to $\{[NNN^{q}]TaCl_3\}$ and $\{[NNN^{q}]Ta(=NNCPh_2)Cl_2\}$, respectively, upon reaction with 0.5 equiv of $PhICl_2$ and Ph_2CN_2, respectively.[7] Iron complexes of bis(imino)pyridine [^{iPr}PDI = 2,6-$(2,6\text{-}^{i}Pr_2C_6H_3N{=}CMe)_2C_5H_3N_3$] undergo both one- and two-electron oxidation reactions, depending on the reaction conditions. For example, Chirik and co-workers have shown

Received: August 15, 2012
Published: October 23, 2012

   dx.doi.org/10.1021/ic301792w | Inorg. Chem. 2012, 51, 11891−11897

that (^{iPr}PDI)Fe(N_2)$_2$ is oxidized by two electrons to afford (^{iPr}PDI)Fe(=NMes) by N_3Mes,[8] and that (^{iPr}PDI)Fe(CO)$_2$ is oxidized by a single electron upon reaction with [Cp_2Fe][BAr^F] [BAr^F = B(C_6H_3-3,5-CF_3)].[9] Cobalt(III) complexes of the redox active ligand amidophenolate (ap^{Ar})$^{2-}$ [ap^{Ar2-} = 2,4-di-*tert*-butyl-6-(phenylamido)phenolate] undergo both one- and two-electron oxidation processes with chlorine-based oxidants depending on the starting oxidation state of the complex.[10]

Examples of ligand-based two-electron redox reactions supported by redox-inactive metal centers include the synthesis of Zr(isq)$_2$(Cl)$_2$ from Cl_2 and Zr(ap)$_2$(THF)$_2$ (isq = 2,4-di-*tert*-butyl-6-*tert*-butyliminosemiquinone, ap = 2,4-di-*tert*-butyl-6-*tert*-butylamindophenolate)[11] and the synthesis of (α-im$_2$)$_2$Zr-(O_2)$_2$ by oxidative addition of molecular oxygen to an α-diimine complex of zirconium [α-im$_2$ = glyoxal-bis(2,6-diisopropylphenyl)imine].[12] However, in both examples it is unknown whether the metal complex or the oxidation reagent dictates the outcome of the reaction as a two-electron process.

As one of many examples of ligand-based oxidation chemistry,[13] we have recently shown that [(IP$^-$)-(IP^{2-})Al(OH)]$^-$ and (IP$^-$)$_2$Al(OH) are formed by one- or two-electron oxidation of M$^+$[(IP^{2-})$_2$Al]$^-$ and that the product identity is dictated by the countercation, M = (DME)$_3$Na or Bu_4N, respectively [IP = 2,6-bis(1-methylethyl)-*N*-2-pyrindinylmethylene)phenylamine].[14] Herein we demonstrate that complexes of the form (IP$^-$)$_2$GaX (X = Cl, OH, TEMPO) and [(IP^{2-})$_2$Ga]$^-$ can be interconverted only via an *overall* two-electron process whether two-electron or one-electron oxidants are employed. We also discuss the origin of this reactivity with relation to the stability of the mixed-valent single electron transfer intermediate as estimated by cyclic voltammetry. Taken together, the foregoing results indicate that the redox chemistry of (IP$^-$)$_2$Ga^{III} is quite distinct from analogous (IP$^-$)$_2$Al^{III} chemistry and is arguably more in line with the redox properties of the platinum group metals, which also undergo *overall* two-electron reactions.

RESULTS AND DISCUSSION

Synthesis of Compounds. The first indication that Ga(III) complexes of IP promote *net* two-electron chemistry was observed upon reaction of M$^+$[(IP^{2-})$_2$Ga]$^-$ (M = Bu_4N, **1a**; (DME)$_3$Na, **1b**) with pyridine *N*-oxide (pyO) in THF solution (Scheme 1). Each reaction was initiated at −78 °C and then

Scheme 1

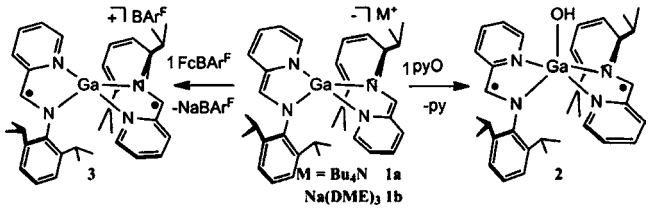

stirred at room temperature for 30 min, during which time the deep purple color of **1** was replaced by a deep green color, typical of the singly reduced ligand in (IP$^-$)$_2$EX complexes (E = Al, Ga, X = anionic ligand).

The IR spectra hinted at formation of (IP$^-$)$_2$Ga(OH) (**2**) as the product, with a sharp band at 3659 cm^{-1} due to the OH functional group (Supporting Information, Table S1).[15] Confirmation of the molecular structure of **2** obtained from each of the reactions came from X-ray diffraction experiments performed on single crystals (vide infra), and the electronic structure of the complex was confirmed by temperature-dependent susceptibility measurements and EPR spectroscopy (Figure 1 and Supporting Information, Figure S1). Experiments

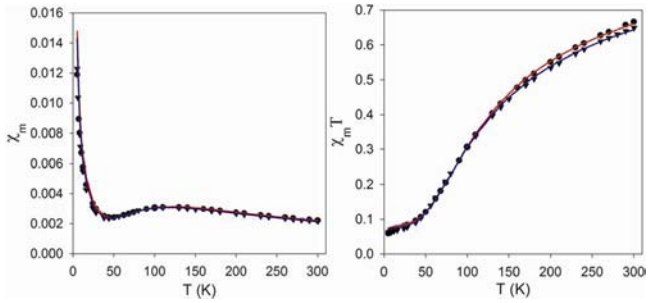

Figure 1. Plot of χ_m vs T (left) and $\chi_m T$ vs T (right) for **2** (●) and **3** (▼) at 1000 Oe from 5 to 300 K. Fit parameters: **2**, g = 2.0, J = −79 cm^{-1}, TIP = 0.19 × 10^{-3} emu, paramagnetic impurity = 5.6%; **3**, g = 2.0, J = −77 cm^{-1}, TIP = 0.15 × 10^{-3} emu, paramagnetic impurity = 7.6%. Fits shown by lines.

performed between 5 and 300 K support a model with two IP$^-$-based ligand radicals coupled antiferromagnetically at low temperature. μ_{eff} = 2.4 μ_B at 300 K, and falls to 0.76 μ_B at 5 K. Moreover, a fit to the data using MAGFIT3.1[16] and a spin Hamiltonian of the form $\hat{H} = -2J\hat{S}_{L(1)}\cdot\hat{S}_{L(2)}$ with g = 2.0, revealed an energy for the interaction J = −79 cm^{-1}. The antiferromagnetic coupling is consistent with the electronic structure of other molecules (IP$^-$)$_2$EX that we have previously reported (where E = Al, Ga, X = anionic ligand).[17]

The origin of the H in the OH functional group of **2** was probed. The reaction of **1a** with pyO occurred cleanly (77% yield) and Bu_3N, presumably liberated by Hoffman elimination after deprotonation of Bu_4N^+, was detected by ^{1}H NMR spectroscopy as evidence for an acid−base reaction for the origin of H$^+$ in the −OH group. Formation of **2** from **1b** was less clean (30% yield), presumably because no readily available proton source was present under the initial reaction conditions. Under these circumstances, the lowered yield for the reaction implies that H is obtained through a ligand degradation pathway. Experiments between **1b** and pyO that were performed in THF-d_8 solution revealed no D incorporation, which ruled out C−H activation of strong C−H bonds as a reaction pathway. We also saw no evidence, using single crystal X-ray analysis or ^{1}H NMR spectroscopy, for C−H activation of the diisopropylphenyl group on the IP ligand.[18] When the reaction of **1b** with pyO was performed in THF with added 1,10-dihydroanthracene, a slight increase in yield of **2** (46%) was observed. We could detect anthracene formation by ^{1}H NMR spectroscopy, and this suggested that in the presence of very weak C−H bonds a transient Na[(IP$^-$)(IP^{2-})Ga−O] intermediate can perform C−H activation before a subsequent second oxidation event occurred.[14,19] We speculate that in the absence of very weak C−H bonds **1b** is oxidized in two sequential one-electron steps to (IP$^-$)$_2$Ga−O$^-$, which is highly basic and goes on to abstract an H$^+$ from the most acidic source available, to form **2**. In either pathway the preference for *overall* two-electron chemistry is driven by the instability of the mixed-valent state.

In contrast to our previous reports on the oxidation chemistry of aluminum,[14] the apparent preference for **1a** and **1b** to undergo net two-electron redox chemistry is noteworthy.

dx.doi.org/10.1021/ic301792w | Inorg. Chem. 2012, 51, 11891−11897

We were interested to discover further examples of this chemistry and to see if net one-electron transformations could be observed. Accordingly, **1a** was reacted with the one-electron outer-sphere oxidant ferrocenium (Fc) using the $FcBAr^F$ salt (Scheme 1). Reaction of **1a** with 2 equiv of $FcBAr^F$ was performed in toluene at −78 °C and afforded, upon workup, deep blue-green-colored $[(IP^-)_2Ga][BAr^F]$ (**3**) in 87% yield. When 1 equiv of $FcBAr^F$ was employed a 1:1 mixture of **1a** and **3** was obtained. Confirmation of the molecular structure of **3** was obtained from X-ray diffraction experiments performed on single crystals of **3** (vide infra), and the electronic structure of the complex was confirmed by temperature-dependent susceptibility measurements (Figure 1). The magnetization measurements indicated that **3** has a biradical electronic structure and that the energy for the antiferromagnetic coupling is best modeled with $J = -77\ cm^{-1}$.

As a further probe of the oxidation pathways for **1b**, we chose an oxidant that could act as either a one- or two-electron oxidant, (2,2,6,6-tetramethylpiperidin-1-yl)oxyl (TEMPO) (Scheme 2). It has been shown by Kira and co-workers and

Scheme 2

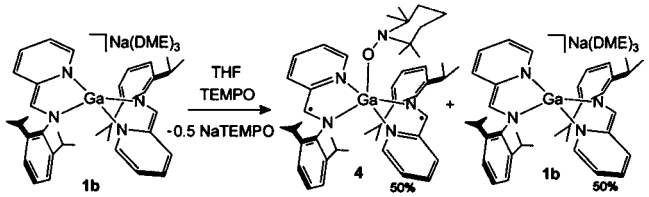

by West and co-workers that main group complexes of TEMPO can be isolated for silicon and germanium.[20] Soper and co-workers have shown that deoxygenation of TEMPO occurs upon two-electron oxidation of rhenium complexes of redox active ligands, while the N−O bond remained intact during one-electron processes.[21] N−O bond cleavage was also observed by Hayton and co-workers in the reaction of TEMPO with uranium(III) complexes in a net two-electron process.[22] Reaction of **1b** with 1 equiv of TEMPO afforded a brown solution, and separation of two gallium-containing products was achieved on the basis of their differences in solubility. The two components were identified as **1b** and $(IP^-)_2Ga(TEMPO)$ (**4**), in addition to NaTEMPO. Again **1b** showed a preference for overall two-electron chemistry; however, similar to the reaction with pyO, it is likely that this reaction proceeds through two one-electron steps rather than a single two-electron step, because the N−O bond of TEMPO remained intact after the reaction. Addition of 2 equiv of TEMPO to **1b** proceeded cleanly to form **4** in much higher yield and left no unreacted **1b** in solution.

We have now described three examples of oxidation reactions in which **1a** or **1b** in combination with one- or two- electron oxidants afford exclusively *net* two-electron-oxidized products. We have previously observed one example of aluminum chemistry where a three-electron reduction of 2 equiv of IP, followed by reaction with $AlCl_3$, results in formation of mixed-valent $[(IP^{2-})Al]_2(\mu\text{-IP-IP}^{2-})$ (Scheme 3).[17] Presumably this reaction passes through a radical intermediate species $(IP^-)(IP^{2-})Al$. We investigated this synthetic strategy using $GaCl_3$ in place of $AlCl_3$, and this reaction afforded a 1:1 mixture of $(IP^-)_2GaCl$ and $[(IP^{2-})_2Ga]^-$ (Scheme 4). Again, the putative $(IP^-)(IP^{2-})Ga$ intermediate, which we expect to

Scheme 3

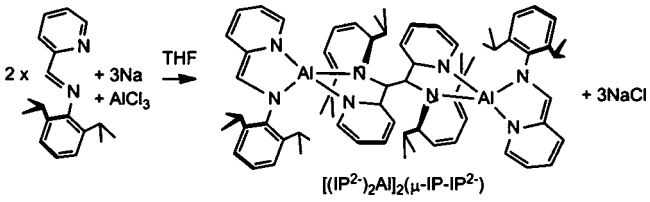

Scheme 4

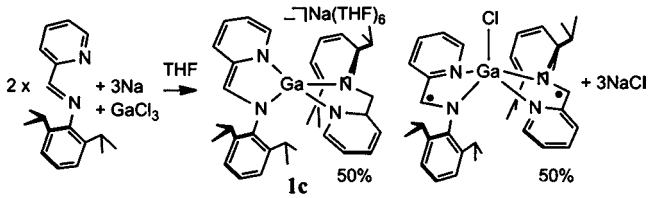

form during the first electron transfer, is less stable than the aluminum analogue and undergoes disproportionation too fast to undergo the carbon−carbon coupling reaction observed in the reaction with aluminum.

Solid-State Structures. The solid-state structure of **2** was confirmed by single crystal X-ray diffraction analysis of a green single crystal grown from a concentrated hexane solution held at −25 °C (Figure 2 and Supporting Information, Tables S2

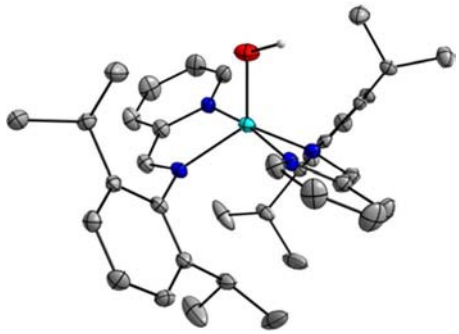

Figure 2. Solid-state structure of **2**. Light blue, gray, blue, red, and white ellipsoids represent Ga, C, N, O, and H atoms, respectively. Ellipsoids are at 50%, and selected H atoms are omitted.

and S3). Compound **2** has a trigonal bipyramidal geometry with $\tau = 0.776$[23] and this is in accord with the other five-coordinate aluminum and gallium complexes of IP that we have previously reported.[17,24,25]

The solid-state structure of **3** was confirmed by single-crystal X-ray diffraction analysis of a blue-green single crystal grown from a concentrated hexane/toluene (1:1) solution held at −25 °C for 1 week (Figure 3 and Supporting Information, Tables S2 and S3). This complex is best described as tetrahedral, although there is a deviation from ideal tetrahedral geometry due to the pinched bite angles of the IP^- chelate ligand. The $N_{py}-Ga-N_{im}$ angle is 86.31(9)°, which is significantly smaller than the expected 104.9°. The $N_{py}-Ga-N_{im}$ angle in **3** is, however, larger than the chelate bite angle that we generally observe for one-electron-reduced IP. For example $N_{py}-Ga-N_{im}$ in **2** is 80.34(5)° and in previously reported $(IP^-)_2GaCl$ is 80.73(5)°.[25] We attribute this result to the shorter $Ga-N_{im}$ and $Ga-N_{py}$ bond lengths that we observe in **3**, which likely

dx.doi.org/10.1021/ic301792w | Inorg. Chem. 2012, 51, 11891−11897

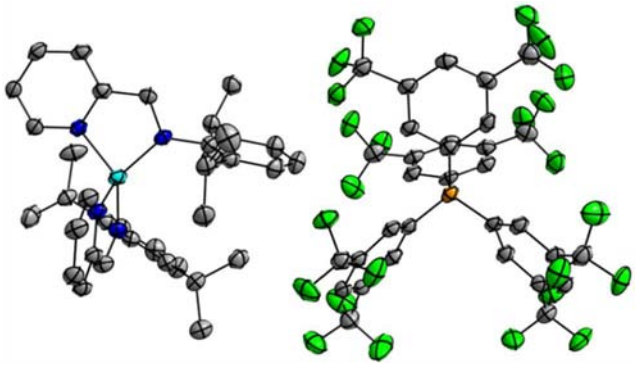

Figure 3. Solid-state structure of **3**. Light blue, gray, blue, green, orange ellipsoids represent Ga, C, N, F, and B atoms, respectively. Ellipsoids are at 50%, and H atoms are omitted.

creates some strain in the IP^- geometry and forces the chelate bite angle to enlarge as described.

The Ga–N_{im} and Ga–N_{py} bond lengths are ~0.10 and 0.13 Å, respectively, shorter than in $(IP^-)_2GaCl$ at 1.875(2) and 1.958(2) Å, respectively. This is most likely because of a greater ionic gallium–ligand interaction in **3** as compared to the interaction in five-coordinate $(IP^-)_2GaCl$ and **2**. The difference in geometry around the metal center in **3** also extends further out into the C, N framework of the ligand. The C_{im}–N_{im} bond lengths, at 1.370(3) Å are ~0.02 Å longer, and the C_{im}– C_{py} bond lengths at 1.429(4) Å are ~0.03 Å shorter, than those in $(IP^-)_2GaCl$ or **2**. These metrics correspond to a slightly "more reduced" IP^- ligand for **3** than in either $(IP^-)_2GaCl$ or **2**.[24,25]

The solid-state structure of **4** was confirmed by single crystal X-ray diffraction analysis of a green single crystal grown from a concentrated hexane solution held at −25 °C (Figure 4 and

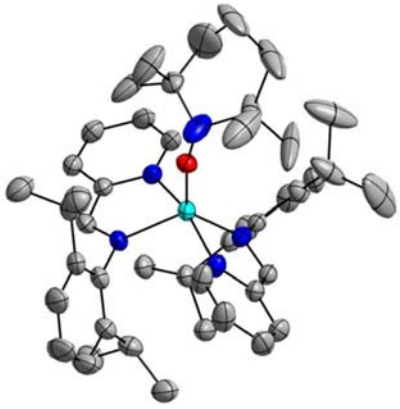

Figure 4. Solid-state structure of $(IP^-)_2Ga(TEMPO)$ in **4**. Light blue, gray, blue, and red ellipsoids represent Ga, C, N, and O atoms, respectively. Ellipsoids are at 50%, and H atoms are omitted. One orientation of the disordered TEMPO ligand is shown.

Tables 2 and 3). Compound **4** has a geometry somewhat distorted from ideal trigonal bipyramidal, as evidenced by the value of τ = 0.662. This value represents one of the lowest τ values we have observed and suggests, on the basis of our previous structural analyses, that the IP^- ligand in **4** should be one of the "least reduced" ligands.[24] The C_{im}–N_{im} and C_{im}–C_{py} bond lengths confirm that IP^- in **4** lies at the least reduced end of one-electron-reduced IP ligands we have observed.

Empirical Explanation for Net Two-Electron Redox Changes Observed with (IP^{n-})Ga(III). The most remarkable feature of the reaction chemistry described herein is that the redox reactivity observed for Ga(III), i.e., the net two-electron redox changes during reactions, is markedly different than the previously observed reactivity of Al(III), i.e., one- or two-electron redox changes depending on reaction conditions.[14] Cyclic voltammetry (CV) is often a useful probe for assessing the thermodynamic stability, and hence the synthetic accessibility, of mixed-valent states. With this in mind, we searched for an explanation for observed differences in reactivity between gallium and aluminum complexes.

Comparison of the CV's of **1b** and the aluminum analog $[(DME)_3Na][(IP^{2-})_2Al]$ showed that the two-electron $(IP^{2-})_2 \leftrightarrow (IP^-)_2$ couple is an unresolved two-electron process for **1b** but is two resolved one-electron couples for the aluminum analog, with 0.19 V spacing (Supporting Information, Figure S2).[17,25] CV measurements of **1b** down to scan rates as slow as 10 mV s^{-1} did not resolve the $(IP^{2-})_2 \leftrightarrow (IP^-)_2$ couple into observable one-electron events.

This does not rule out the likely situation that two successive one-electron events are occurring, but it does demonstrate that these events are faster for gallium than for aluminum. Furthermore, these electrochemical observations predict the behavior we observed in synthetic chemistry experiments (vide supra). However, they do not explain *why* electronic coupling through aluminum is apparently more effective than through gallium.

The mixed-valent aluminum complex, $[(IP^-)\{(THF)(DME)NaIP^{2-}\}Al(OH)]$ is five-coordinate, so we thought that the stability of this complex, due to the strength of electronic coupling between ligands, might be assessed using the same metrical parameters as we have previously used to assess the electronic coupling in five-coordinate biradical complexes of aluminum.[24] Indeed, $[(IP^-)\{(THF)(DME)NaIP^{2-}\}Al(OH)]$ falls on the same linear plot of ΔE versus dihedral angle that we previously reported for a series of five-coordinate aluminum complexes of the form $(IP^-)_2AlX$ (Figure 5, blue point). As previously reported, in the series of aluminum

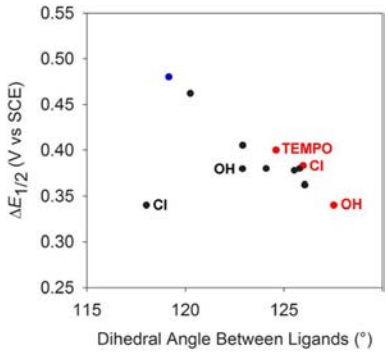

Figure 5. Plot of ΔE versus dihedral angle for five-coordinate complexes of Al and Ga. $(IP^-)_2AlX$ are black points, $(IP^-)_2GaX$ are red points, and $[(IP^-)\{(THF)(DME)NaIP^{2-}\}Al(OH)]$ is a blue point.[26]

complexes (black dots in Figure 5), the X ligand was varied and this resulted in changes to the complex geometry and ΔE for the reaction $(IP^-)_2AlX + (IP)_2AlX \leftrightarrow (IP^-)(IP)AlX$. Specifically, as the dihedral angle between the planes defined by N_{im}–C_{im}–C_{py}–N_{py} became larger (Chart 1), ΔE became smaller. We speculated that this effect resulted from a weakened

dx.doi.org/10.1021/ic301792w | *Inorg. Chem.* 2012, 51, 11891–11897

interaction of the IP π system with the Al−X σ^* orbital as the dihedral angle becomes more obtuse.[24]

Chart 1[27]

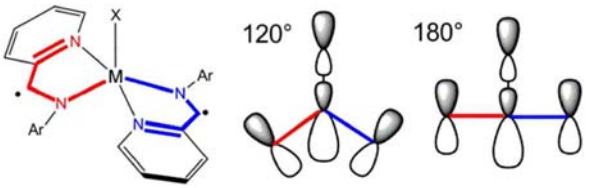

Of significance to the current work, we compared the geometrical parameters of gallium complexes of the form $(IP^-)_2GaX$ to the aluminum complexes. Notably, all gallium complexes of the form $(IP^-)_2GaX$ have larger dihedral angles than the corresponding aluminum complexes. For example, the dihedral angles in $(IP^-)_2AlCl$ and $(IP^-)_2Al(OH)$ are 118.03(8)° and 122.90(7)°, and for the corresponding gallium complexes, **2** and **4**, they are 127.54(9)° and 124.61(6)°, respectively. This observation can be rationalized by the fact that the ionic radius of Ga(III) is 62 pm compared with Al(III) at 53 pm.[28] We speculate that the larger ionic radius of Ga(III) results in a larger dihedral angle in five-coordinate complexes of Ga(III) and that this in turn would reduce the extent of electronic coupling between the IP ligands, as compared with aluminum complexes. Indeed the ΔE values for **2**, **4** (Figure 6 and Supporting Information, Table S4), and previously reported $(IP^-)_2GaCl$ compare favorably with the previously reported aluminum complexes falling on the same trend line in Figure 5.

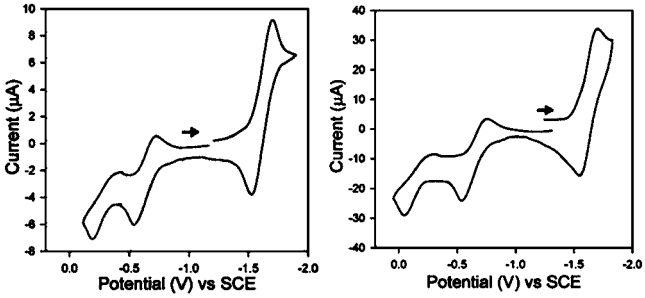

Figure 6. CV's for **2** (left) and **4** (right), in 0.3 M Bu_4NPF_6 THF solution. GC electrode. Scan rate = 100 mV/s.

The differences in energies in the metal frontier orbitals may also contribute to diminished coupling in the Ga complexes. It has been previously observed that the heavier group 13 elements form weaker metal halide bonds due to decreased covalency in the metal−halide bond stemming from the inert pair effect.[29] This decrease in bond strength presumably correlates with a less prominent E−X σ^* orbital and thus a decrease in overlap with the ligand π system, and a decrease in electronic coupling may be expected. Future work, using theoretical methods, will probe the significance of these effects.

CONCLUSIONS

We have shown that gallium(III) complexes of IP promote exclusively *net* two-electron redox transformations between the $(IP^-)_2GaX$ and $[(IP^{2-})_2Ga]^-$ oxidation states. The observed two-electron redox changes are very likely successive one-electron redox changes, which occur in quick succession due to the thermodynamic instability of the mixed-valent $(IP^{2-})(IP^-)$ oxidation state in five-coordinate gallium complexes. We have no evidence to suggest that these redox reactions proceed via two-electron event. Regardless of the electron transfer mechanism, these reactions afford two-electron changes on the gallium complexes. We have also proposed that the instability of the mixed-valent state stems from the larger ionic radius of Ga(III), which leads to larger dihedral angles between the planes of the IP ligand π systems for gallium complexes as compared with aluminum complexes. We proposed that the more obtuse angle resulted in decreased overlap between the IP π system and the E−X σ^* orbital. Future theoretical work will probe the significance of electronic effects, such relative energies of the frontier orbitals, to the strength of electronic coupling.

EXPERIMENTAL SECTION

Physical Measurements. Elemental analyses were performed by Columbia Analytical. ^{1}H NMR spectra were recorded at ambient temperature using a Varian 400 MHz spectrometer. Chemical shifts were referenced to residual solvent. The paramagnetic compounds **2**−**4** were NMR-silent. Electrochemical measurements were recorded in a glovebox under a dinitrogen atmosphere using a CH Instruments Electrochemical Analyzer, a glassy carbon working electrode, a platinum wire auxiliary-electrode, and an $Ag/AgNO_3$ nonaqueous reference electrode. Reported potentials are all referenced to the SCE couple, and were determined using decamethylferrocene as an internal standard. The number of electrons passed in a given redox process was estimated by comparison of the peak current with the peak current of decamethylferrocene included as an internal standard. UV−vis−NIR spectra were recorded in THF solutions using a Lambda 750 UV−vis−NIR spectrophotometer. Magnetic measurements were recorded using a Quantum Designs MPMS XL magnetometer at 0.1 T. The sample was contained under nitrogen in a gelcap and suspended in the magnetometer in a plastic straw. The magnetic susceptibility was adjusted for diamagnetic contributions using the constitutive corrections of Pascal's constants. EPR measurements were performed on 100 μL dilute solutions of the compound loaded into 4 mm OD quartz tubes in a glovebox and then freeze−pump−thawed and flame-sealed on a Schlenk line. X-band continuous-wave EPR measurements were performed at the CalEPR center at UC Davis, with a Bruker ECS106 X-band spectrometer equipped with a Bruker SHQ resonator, an EIP 548A frequency counter, and an Oxford liquid-helium cryostat. The magnetic field was calibrated with a Bruker ER036TM teslameter.

X-ray Structure Determinations. X-ray diffraction studies were carried out on a Bruker SMART 1000, a Bruker SMART APEXII, and a Bruker SMART APEX Duo diffractometer equipped with a CCD detector.[30] Measurements were carried out at −175 °C using Mo Kα (λ = 0.710 73 Å) and Cu Kα (λ = 1.5418 Å) radiation. Crystals were mounted on a glass capillary or Kaptan Loop with Paratone-N oil. Initial lattice parameters were obtained from a least-squares analysis of more than 100 centered reflections; these parameters were later refined against all data. Data were integrated and corrected for Lorentz polarization effects using SAINT and were corrected for absorption effects using SADABS2.3.

Space group assignments were based upon systematic absences, E statistics, and successful refinement of the structures. Structures were solved by direct methods with the aid of successive difference Fourier maps and were refined against all data using the SHELXTL 5.0 software package. Thermal parameters for all non-hydrogen atoms were refined anisotropically. Hydrogen atoms, where added, were assigned to ideal positions and refined using a riding model with an isotropic thermal parameter 1.2 times that of the attached carbon atom (1.5 times for methyl hydrogens).

Preparation of Compounds. All manipulations were carried out using standard Schlenk or glovebox techniques under a dinitrogen atmosphere. Unless otherwise noted, solvents were deoxygenated and dried by thorough sparging with Ar gas followed by passage through

dx.doi.org/10.1021/ic301792w | Inorg. Chem. 2012, 51, 11891−11897

an activated alumina column. Deuterated solvents were purchased from Cambridge Isotopes Laboratories, Inc. and were degassed and stored over activated 3 Å molecular sieves prior to use. The iminopyridine ligand (IP),[31] $[Bu_4N][(IP^{2-})_2Ga]$ (**1a**), $[(DME)_3Na][(IP^{2-})_2Ga]$ (**1b**),[25] and $(IP^{-})_2AlOH$,[14] were prepared according to previously reported procedures. $FcBAr^F$ was prepared according to the previously reported procedure for $FcPF_6$.[32] Pyridine *N*-oxide was purified by vacuum sublimation prior to use. All other reagents were purchased from commercial vendors and used as received.

$(IP^{-})_2Ga(OH)$ (2). A solution of pyridine *N*-oxide (0.06 g, 0.60 mmol) in THF (5 mL) was added to a stirred solution of **1a** (0.50 g, 0.56 mmol) in THF (5 mL) and the reaction solution was stirred for 15 min. The resulting dark green solution was evaporated to dryness, dissolved in hexanes (20 mL), and filtered through Celite. The volume of solution was reduced to 10 mL and cooled at −25 °C to afford **2** as a dark green powder (0.28 g, 77%). Crystals suitable for X-ray diffraction were obtained from cooling a saturated hexanes solution at −25 °C for 4 days. IR (KBr): 3659 (m, OH), 1586 (m, C_{im}–N_{im}) cm^{-1}. UV−vis spectrum (THF) λ_{max} (ε_M): 242 (29 200), 362 (27 100), 426 (6900), 455 (6800), 691 (br, 2000) nm (L mol^{-1} cm^{-1}). Anal. Calcd for $C_{36}H_{45}GaN_4O$: C, 69.80; H, 7.32; N, 9.04. Found: C, 70.03; H, 7.55; N, 8.85. μ_{eff} = 2.3 μ_B at 300 K.

$[(IP^{-})_2Ga][BAr^F]$ (3). A suspension of $FcBAr^F$ (1.05 g, 1.0 mmol) in 10 mL of toluene was added to a solution of **1a** (0.42 g, 0.5 mmol) in toluene cooled at −78 °C. In order to prevent overoxidation, the oxidant was titrated into the solution of **1a** and addition was stopped when the reaction mixture was a uniform green color. The resulting green suspension was filtered through Celite to remove salts. The solution was concentrated to 5 mL and then 10 mL of hexanes was layered on top. After cooling at −25 °C overnight, **3** was obtained as a blue-green powder (1.27 g, 87%). Crystals suitable for X-ray diffraction were grown by cooling a concentrated hexane/toluene (1:1) solution at −25 °C for 1 week. IR (KBr): 1592 (sh, C_{im}–N_{im}) cm^{-1}. UV−vis spectrum (THF) λ_{max} (ε_M): 362 (35 100), 421 (11 500), 655 (br, 3200) nm (L mol^{-1} cm^{-1}). Anal. Calcd for $C_{68}H_{56}BF_{24}GaN_4$: C, 55.72; H, 3.85; N, 3.82. Found: C, 55.98; H, 4.02; N, 3.66. μ_{eff} = 2.3 μ_B at 300 K.

Reaction of 1a with $FcBAr^F$ (1:1). A suspension of $FcBAr^F$ (0.53 g, 0.5 mmol) in 5 mL of THF was added to a solution of **1a** (0.45 g, 0.5 mmol) in 5 mL of THF at −25 °C. The resulting brown solution was stirred for 1 h. Due to similarities in the solubility of **3** and **1a**, the two products could not be separated from each other. NaOH (10 mg, 0.25 mmol) was added to the solution, which was stirred for an additional 1 h. The solution was evaporated to dryness and the resulting residue extracted into hexane to afford a green solution and a dark purple precipitate. The green solution was dried in a vacuum and the resulting green powder (0.11 g, 37%) was confirmed as $(IP^{-})_2GaOH$ (**2**) by IR spectroscopy [IR (KBr): 3659 (m, OH), 1586 (m, C_{im}–N_{im}) cm^{-1}]. The purple solid was washed with an additional 20 mL of hexane and then extracted into DME. The solution was filtered through Celite to remove salts. The resulting solution was evaporated to dryness and the resulting purple powder (0.22 g, 41%) was confirmed to be previously reported $[Na(THF)_6][(IP^{2-})_2Ga]$ using ^1H NMR spectroscopy.[25]

$(IP^{-})_2Ga(TEMPO)$ (4). A solution of TEMPO (0.16 g, 1.0 mmol) in THF (5 mL) was added to a stirred solution of **1b** (0.87 g, 1.0 mmol) in THF (5 mL). The resulting brown solution was evaporated to dryness and extracted into hexane (20 mL). The solution was filtered through Celite to remove unreacted **1b** and salts. The green filtrate was concentrated to 10 mL and cooled at −25 C° for 3 days to afford **4** as a green powder (0.20 g, 26%). Extraction of the **1b** and NaTEMPO portion into benzene gave a purple solution and white precipitate. The purple solution was evaporated to dryness to afford **1b** (0.25 g, 28%). If the same reaction was run with 2 equiv of TEMPO, then 0.59 g (76%) of **4** was obtained, and no unreacted **1b** remained. Crystals suitable for X-ray diffraction were grown by chilling a concentrated hexane solution at −25 °C for 1 week. IR (KBr): 1591 (s, C_{im}–N_{im}) cm^{-1}. UV−vis spectrum (THF) λ_{max} (ε_M): 360 (32 400), 423 (10 600), 672 (br, 2500) nm (L mol^{-1} cm^{-1}). Anal. Calcd for $C_{45}H_{62}GaN_5O$: C, 71.24; H, 8.24; N, 9.23. Found: C, 71.33; H, 8.47; N, 9.14. The fraction that was not soluble in hexane was analyzed by ^1H NMR and found to match the spectrum of **1b** and NaTEMPO.

Reaction of 2IP, $GaCl_3$, and 3Na. Sodium metal (0.20 g, 8.70 mmol) and IP (1.50 g, 5.64 mmol) were stirred in DME for 2 h. $GaCl_3$ (0.50 g, 2.84 mmol) was added and allowed to stir for 24 h. The resulting brown solution was filtered through Celite to remove salts and evaporated to dryness. The residue was extracted into hexanes and filtered to obtain a purple solid and a green filtrate. The purple solid was dissolved in THF (5 mL), hexanes were layered on top, and the reaction was cooled at −25 °C for 3 days to give $[Na(THF)_6][(IP^{2-})_2Ga]$ as a solid purple powder (0.31 g). The green filtrate was concentrated to 5 mL and cooled at −25 °C overnight. The green precipitate was collected by filtration and confirmed by IR and UV−vis to be previously reported[19] $(IP^{-})_2GaCl$ (0.11 g). Green material: IR (KBr): 1586 (m, C_{im}–N_{im}) cm^{-1}. UV−vis spectrum (THF) λ_{max} (ε_M): 240 (16 028) 362 (7779) 708 (2110) nm (L mol^{-1} cm^{-1}). Purple material: ^1H NMR (400 MHz, C_6D_6): 7.32 (br, 2H, ph), 7.25 (br, 4H, Ph), 6.90 (d, *J* = 6.52, 2H, py), 5.98 (d, *J* = 9.60, 2H, py), 5.63 (s, 2H, imC*H*), 5.46 (br, 2H, py), 4.71 (t, *J* = 6.50, 2H, py), 4.41 (m, 2H, C*H*$(CH_3)_2$), 3.45 (m, 2H, C*H*$(CH_3)_2$), 2.79 (s, 24H, THF), 1.97 (d, *J* = 7.14, 6H, CH(C*H*$_3$)$_2$), 1.59 (d, *J* = 7.14, 6H, CH(C*H*$_3$)$_2$), 1.46 (d, *J* = 7.14, 6H, CH(C*H*$_3$)$_2$), 0.61 (d, *J* = 7.14, 6H, CH(C*H*$_3$)$_2$). UV−vis spectrum (THF) λ_{max} (ε_M): 245 (21 413) 362 (7560) nm (L mol^{-1} cm^{-1}).

■ ASSOCIATED CONTENT

Ⓢ Supporting Information

IR data, EPR spectra, CV's, CIF files. This material is available free of charge via the Internet at http://pubs.acs.org/.

■ AUTHOR INFORMATION

Corresponding Author

*E-mail: laberben@ucdavis.edu.

Author Contributions

‡These authors contributed equally.

Notes

The authors declare no competing financial interest.

■ ACKNOWLEDGMENTS

We thank the University of California—Davis and the Alfred P. Sloan Foundation for support of this work and the National Science Foundation (Grant 0840444) for a dual source X-ray diffractometer. T.W.M. thanks UC Davis for a 2012 Summer Graduate Research Fellowship.

■ REFERENCES

(1) For example: (a) Crabtree, R. H. *The Organometallic Chemistry of the Elements*, 5th ed.; John Wiley & Sons, Inc.: Hoboken, NJ, 2009. (b) Hartwig, J. F. *Organotransition Metal Chemistry—From Bonding to Catalysis*; University Science Books: Sausalito, CA, 2010.

(2) (a) Power, P. P.; Gabbaï, F. P. *Inorg. Chem.* **2011**, *50*, 12221. (b) Jeong, J. U.; Tao, B.; Sagasser, I.; Henniges, H.; Sharpless, K. B. *J. Am. Chem. Soc.* **1998**, *120*, 6844. (c) Stephan, D. W. *Org. Biomol. Chem.* **2008**, *6*, 1535.

(3) Hardman, N. J.; Power, P. P. *Inorg. Chem.* **2001**, *40*, 2474.

(4) Roesky, H. W.; Kumar, S. S. *Chem. Commun.* **2005**, 4027.

(5) Hardman, N. J.; Cui, C.; Roesky, H. W.; Fink, W. H.; Power, P. P. *Angew. Chem., Int. Ed.* **2001**, *40*, 2172.

(6) Zhu, H.; Chai, J.; Chandrasekhar, V.; Roesky, H. W.; Magull, J.; Vidovic, D.; Schmidt, H. G.; Noltemeyer, M.; Power, P. P.; Merrill, W. A. *J. Am. Chem. Soc.* **2004**, *126*, 9472.

(7) Nguyen, A. I.; Blackmore, K. J.; Carter, S. M.; Zarkesh, R. A.; Heyduk, A. F. *J. Am. Chem. Soc.* **2009**, *131*, 3307.

(8) Bart, S. C.; Lobkovsky, E.; Bill, E.; Chirik, P. J. *J. Am. Chem. Soc.* **2006**, *128*, 5302.

(9) Tondreau, A. M.; Milsmann, C.; Lobkovsky, E.; Chirik, P. J. *Inorg. Chem.* **2011**, *50*, 9888.
(10) (a) Smith, A. L.; Clapp, L. A.; Hardcastle, K. I.; Soper, J. D. *Polyhedron* **2010**, *29*, 164. (b) Smith, A. L.; Hardcastle, K. I.; Soper, J. D. *J. Am. Chem. Soc.* **2010**, *132*, 14358.
(11) Blackmore, K. J.; Ziller, J. W.; Heyduk, A. F. *Inorg. Chem.* **2005**, *44*, 5559.
(12) Stanciu, C.; Jones, M. E.; Fanwick, P. E.; Abu-Omar, M. M. *J. Am. Chem. Soc.* **2007**, *129*, 12400.
(13) For example (a) Lu, C. C.; DeBeer George, S.; Weyhermüller, T.; Bill, E.; Bothe, E.; Wieghardt, K. *Angew. Chem., Int. Ed.* **2008**, *47*, 6348. (b) Sylvester, K. T.; Chirik, P. J. *J. Am. Chem. Soc.* **2009**, *131*, 8772. (c) Hameline, M. R.; Heyduk, A. H. *J. Am. Chem. Soc.* **2006**, *128*, 8410.
(14) Myers, T. W.; Berben, L. A. *J. Am. Chem. Soc.* **2011**, *133*, 11865.
(15) Previously reported imine spectra: Kincaid, K.; Gerlach, C. P.; Giesbrecht, G. R.; Hagadorn, J. R.; Whitener, G. R.; Shafir, A.; Arnold, J. *Organometallics* **1999**, *18*, 5360.
(16) Schmitt, E. A. Ph.D. Thesis, University of Illinois Urbana–Champaign, Urbana, IL. 1995.
(17) Myers, T. W.; Kazem, N.; Stoll, S.; Britt, R. D.; Shanmugam, M.; Berben, L. A. *J. Am. Chem. Soc.* **2011**, *133*, 8662.
(18) (a) Atienza, C. C. H.; Bowman, A. C.; Lobkovsky, E.; Chirik, P. J. *J. Am. Chem. Soc.* **2012**, *132*, 16343. (b) Zhu, H.; Chai, J.; Chandrasekhar, V.; Roesky, H. W.; Magull, J.; Vidovic, D.; Schmidt, H. G.; Noltemeyer, M.; Power, P. P.; Merrill, W. A. *J. Am. Chem. Soc.* **2004**, *126*, 9472.
(19) The single or double deprotonation of 1,10-dihydroanthracene is known only to produce anthracene in the presence of strong electrophiles or hydride acceptors and was therefore ruled out as a possible mechanism: (a) Stamm, H.; Lin, P.; Sommer, A.; Woderer., A. *Tetrahedron.* **1989**, *45*, 2571. (b) Kitamura, M.; Shen, B.; Lui, Y.; Zheng, H.; Takahasi, T. *Chem. Lett.* **2001**, 646.
(20) (a) Kira, M.; Ishida, S.; Iwamoto, T.; Kabuto, C. *J. Am. Chem. Soc.* **1999**, *121*, 9722. (b) Naka, A.; Hill, N. J.; West, R. *Organometallics* **2004**, *23*, 6330.
(21) Lippert, C. A.; Soper, J. D. *Inorg. Chem.* **2010**, *49*, 3682.
(22) Fortier, S.; Kaltsoyannis, N.; Wu, G.; Hayton, T. W. *J. Am. Chem. Soc.* **2011**, *133*, 14224.
(23) Addison, A. W.; Rao, T. N.; Reedijk, J.; Van Rijn, J.; Verschoor, G. C. *J. Chem. Soc., Dalton Trans.* **1984**, 1349.
(24) Myers, T. W.; Holmes, A. L.; Berben, L. A. *Inorg. Chem.* **2012**, *51*, 8997.
(25) Kowolik, K.; Shanmugam, M.; Myers, T. W.; Cates, C. D.; Berben, L. A. *Dalton Trans.* **2012**, 7969.
(26) The $(IP^{-})_2AlCl$ species fell well off the trend and exhibited unusual magnetic coupling as well. The origin of this anomalous behavior is under investigation.
(27) Only one orbital in the ligand ring plane is shown, for clarity.
(28) Atkins, P. W. *Physical Chemistry*, 5th ed.; Oxford University Press: Oxford, 1994; p C24.
(29) (a) Drago, R. S. *J. Phys. Chem.* **1958**, *62*, 353. (b) Schwerdfeger, P.; Heath, G. A.; Dolg, M.; Bennett, M. A. *J. Am. Chem. Soc.* **1992**, *114*, 7518.
(30) (a) *SMART Software Users Guide, Version 5.1*; Bruker Analytical X-ray Systems, Inc.: Madison, WI, 1999. (b) *SAINT Software Users Guide, Version 7.0*; Bruker Analytical X-Ray Systems, Inc.: Madison, WI, 1999. (c) Sheldrick, G. M. *SADABS, Version 2.03*; Bruker Analytical X-Ray Systems, Inc.: Madison, WI, 2000. (d) Sheldrick, G. M. *SHELXTL, Version 6.12*; Bruker Analytical X-Ray Systems, Inc.: Madison, WI, 1999. (e) *International Tables for X-ray Crystallography*; Dordrecht: Kluwer Academic Publishers, 1992; Vol. *C*.
(31) Laine, T. V.; Klinga, M.; Leskelä, M. *Eur. J. Inorg. Chem.* **1999**, 959.
(32) Connelly, N. G.; Geiger, W. E. *Chem. Rev.* **2006**, *96*, 877.